Inorganic Chemistry

pubs.acs.org/IC

Article

Design, Synthesis, and Anticancer Studies of a *p*-Cymene-Ru(II)-Curcumin Organometallic Conjugate Based on a Fluorescent 4-Amino-1,8-naphthalimide Tröger's Base Scaffold

Binduja Mohan, Sandra Estalayo-Adrián, Deivasigamani Umadevi, Bjørn la Cour Poulsen, Salvador Blasco, Gavin J. McManus, Thorfinnur Gunnlaugsson,* and Sankarasekaran Shanmugaraju*

Cite This: *Inorg. Chem.* 2022, 61, 11592−11599

Read Online

ACCESS | Metrics & More | Article Recommendations | Supporting Information

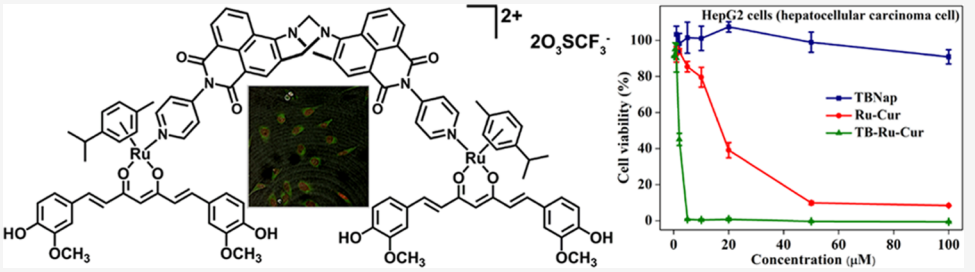

ABSTRACT: A unique V-shaped "chiral" supramolecular scaffold, *N*-(4-pyridyl)-4-amino-1,8-naphthalimide Tröger's base (**TBNap**), was synthesized in good yield from a precursor *N*-(4-pyridyl)-4-amino-1,8-naphthalimide (**Nap**). **TBNap** was characterized using different spectroscopic methods and the molecular structure was elucidated by diffraction analysis. A new *p*-cymene-Ru(II)-curcumin conjugate (**TB-Ru-Cur**) was designed by reacting **TBNap** dipyridyl donor and ruthenium-curcuminato acceptor [**RuCur** = (*p*-cymene)Ru-(curcuminato)Cl] in the presence of silver triflate. **TB-Ru-Cur** was isolated in quantitative yield and characterized using Fourier transform infrared (FT-IR), NMR (^{1}H, ^{13}C, and ^{19}F), and electrospray ionization mass spectrometry (ESI-MS), and the molecular structure has been predicted using a computational study. Both **TBNap** and **TB-Ru-Cur** exhibited intramolecular charge transfer (ICT)-based fluorescence emission. Furthermore, the anticancer properties of **TBNap**, **Ru-Cur**, and **TB-Ru-Cur** were assessed in different cancer cell lines. Gratifyingly, the conjugate **TB-Ru-Cur** displayed fast-cellular internalization and good cytotoxicity against HeLa, HCT-116, and HepG2 cancer cells and the estimated IC_{50} value was much lower than that of the precursors (**TBNap** and **Ru-Cur**) and the well-known chemotherapeutic drug cisplatin.

INTRODUCTION

The design and synthesis of therapeutically active new organic ligands and metal complexes for cancer treatment is an active interdisciplinary field of research.[1,2] While significant achievements have been made to date, it remains that the early-stage detection and effective treatment of cancer are still challenging, particularly because of multidrug resistance and the limited availability of cancer-targeting theragnostic agents.[3,4] Hence, there exists the need to develop novel candidates to overcome such drawbacks. Metal complexes have prominent significance for cancer chemotherapy as metal ions are crucial for several biological processes.[5] In particular, luminescent transition-metal complexes have been identified as promising theragnostic probes, such as Ru(II)−polypyridyl complexes, because of their facile synthesis, easy structural modifications, and functional tunability.[6] Furthermore, complexes such as cisplatin and its derivatives oxaliplatin and carboplatin are well-known Pt(II)-based cancer drugs widely used to effectively inhibit several types of cancer cell growth.[7] However, poor selectivity, dose-dependent toxicity, and multidrug resistance limit their long-term usage for cancer treatments.[8] Recently, ruthenium metal complexes have emerged as a viable substitute to Pt(II)-based metallodrugs because of their comparable ligand-exchange kinetics. As of now, three ruthenium metal complexes, namely, NAMI-A, KP1019, and (N)KP1339, are in clinical observations.[9,10]

Recently, arene-Ru(II) organometallic complexes have been realized for their anticancer properties because of their high solubility, easy functionalization, and improved cancer selectivity.[11−14] Further, the arene-capping unit helps to maintain the structural stability of complexes under various physiological conditions.[14] Some known examples are [(C_6H_5Ph)Ru-(ethylenediamine)Cl][PF_6] (RM175) and [(*p*-

Received: March 26, 2022
Published: July 20, 2022

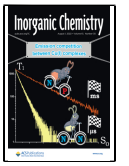

https://doi.org/10.1021/acs.inorgchem.2c01005
Inorg. Chem. 2022, 61, 11592−11599

cymene)Ru(1,3,5-triaza-7-phosphotricyclo[3.3.1.1]-decane)-Cl_2] (RAPTA-C).[15,16] These complexes selectively inhibit metastasis in vivo and exhibit poor in vitro anticancer activity. Nevertheless, the functionalization of such arene-Ru(II) complexes with therapeutically known bioactive ligands would enhance the antitumor efficacy.[7,17] Curcumin is a naturally available bioactive ligand that is extracted from the plant *Curcuma longa* (turmeric) and is famous for its various medicinal properties such as anti-inflammatory, anti-Alzheimer's disease effect, antitumoral effect, antiviral property, and so on.[17−21] Considering the anticancer properties of curcumin, the **Ru-Cur** complex was developed by reacting the commercial curcumin powder with $[(p\text{-cymene})RuCl_2]_2$ in methanol.[22] It has been demonstrated that **Ru-Cur** is an effective anticancer agent against ovarian A2780 (IC_{50} = 23.4 μM) and breast MCF7 (IC_{50} = 19.6 μM) cancer cell lines. Later, the **Ru-Cur** complex was modified by replacing the ancillary chloride with the 1,3,5-triaza-7-phosphaadamantane ligand to enhance the cytotoxic action against A2780R and A2780 ovarian carcinoma cell lines.[23] We have developed several Ru(II)-based luminescent metal complexes and organometallic conjugates based on **TBNap** and demonstrated their anticancer properties against different cancer cell lines.[24−26]

TBNaps are strongly emissive due to the "push−pull" type of intramolecular charge transfer (ICT) transition and their unique cleft-shaped structure, making them an attractive building block in supramolecular chemistry.[25,26] We have developed a plethora of **TBNap** structures and successfully employed them as bifunctional scaffolds to generate multifunctional supramolecular structures, functional materials, and porous polymers for applications in biomedicine and environmental sciences.[26−33] For instance, these have been used as imaging probes for live-cell staining, DNA targeting agents,[24,27,28] and fluorescence sensors for chemical explosives and biologically important analytes.[32] In this article, we report a new **TBNap**-based luminescent *p*-cymene-Ru(II) conjugate (**TB-Ru-Cur**) (see Scheme 1) and demonstrated its anticancer properties in different cancer lines. We foresaw that the cationic nature of **TB-Ru-Cur** would facilitate fast-cellular uptake, and it was found to be the case. The anticancer activity of **TB-Ru-Cur** was checked in HeLa, HCT-116, and HepG2 cancer cell lines, and cell viability studies established the high anticancer activity for **TB-Ru-Cur**, which is significantly prominent than **Ru-Cur** and **TBNap** precursors, and much more potent than cisplatin drug. These results demonstrate the importance of combining multiple anticancer ligands within **TB-Ru-Cur**.

Scheme 1. Synthesis of TB-Ru-Cur

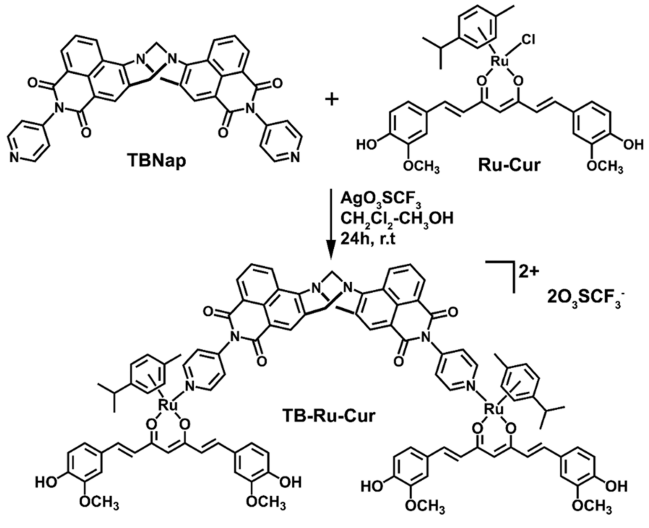

EXPERIMENTAL SECTION

Synthesis of TBNap. *N*-(4-Pyridyl)-4-amino-1,8-naphthalimide (**Nap**, 200 mg, 0.69 mmol, 1 equiv) and paraformaldehyde (31 mg, 1.04 mmol, 1.5 equiv) were taken in a 50 mL round-bottom flask. Trifluoroacetic acid (TFA, 4 mL) was added at 0 °C and the mixture was stirred at room temperature for 12 h under N_2 atmosphere. The reaction mixture was neutralized by adding NH_4OH (100 mL) until a pH > 10 was reached. The organic layer was extracted in dichloromethane (DCM) (200 mL) and washed with saturated $NaHCO_3$ (2 × 100 mL), brine (2 × 100 mL), and H_2O (2 × 100 mL). The solution was dried over $MgSO_4$ and the solvents were removed and triturated with cold diethyl ether to isolate **TBNap** (230 mg, 0.37 mmol, 54%). Anal. calcd (%) for $C_{37}H_{22}N_6O_4.CH_2Cl_2$: C, 65.24; H, 3.46; N, 12.01. Found: C, 65.73; H, 3.62; N, 11.79. Melting point: 319−321 °C (decomp.). HRMS (APCI) *m*/*z*: calcd for $C_{37}H_{23}N_6O_4$ [M + H$^+$] 615.1775, found 615.1760; ^{1}H NMR (400 MHz, $(CD_3)_2SO$) δ 8.82−8.80 (2H, d, J = 8.0 Hz, Ar−H), 8.74−8.72 (4H, d, J = 8.0 Hz, pyridyl-H$_\alpha$), 8.52−8.50 (2H, d, J = 8.0 Hz, Ar−H), 8.16 (2H, s, Ar−H), 8.03−7.99 (2H, t, J = 8.0 Hz, Ar−H), 7.42−7.40 (4H, d, J = 8.0 Hz, pyridyl-H$_\beta$), 5.25−5.20 (2H, d, J = 20.0 Hz, NCH_2), 4.79 (2H, s, NCH_2), 4.74−4.69 (2H, d, J = 20.0 Hz, NCH_2); ^{13}C NMR (101 MHz, $(CD_3)_2SO$) δ 150.56, 148.38, 143.91, 130.76, 130.38, 129.49, 128.00, 127.22, 126.81, 126.23, 124.57, 122.79, 117.90, 64.90, 56.91, 54.90, 15.15; FT-IR υ_{max} (ATR, cm^{-1}) 3326, 31.62, 3053, 2163, 1699, 1666, 1586, 1572, 1507, 1459, 1405, 1356, 1300, 1244, 1188, 1126, 1088, 1038, 931, 781, 691, 659, 626, 587.

Synthesis of TB-Ru-Cur. A mixture of **Ru-Cur** (30 mg, 0.047 mmol, 2 equiv) and $AgCF_3SO_3$ (13 mg, 0.052 mmol, 2.2 equiv) was stirred in 1:1 DCM-CH_3OH (8 mL) at room temperature for 1 h in dark and then filtered through celite to remove AgCl. **TBNap** (14 mg, 0.023 mmol, 1.0 equiv) was added to the filtrate, which was stirred overnight at room temperature. Then, the reaction mixture was filtered and the solvent was stripped under vacuum. The residue was redissolved in 3 mL of DCM-CH_3OH (1:1) and diethyl ether was slowly diffused to isolate the product **TB-Ru-Cur** (20 mg, 0.011, 48%) as an orange-brown solid. Anal. calcd (%) for $C_{101}H_{88}F_6N_6O_{22}Ru_2S_2{\cdot}6CH_2Cl_2$: C, 48.91; H, 3.84; N, 3.20. Found: C, 48.93; H, 3.52; N, 3.17. Melting point: 285−288 °C (decomp.); HRMS (ESI$^+$) calcd for [M − (RuCur + $SO_3CF_3^-$)]$^+$ *m*/*z* = 1217.3036 ($C_{68}H_{55}N_6O_{10}Ru$), found *m*/*z* = 1217.3016. ^{1}H NMR (400 MHz, $CDCl_3$−CD_3OD) δ 9.24−9.22 (d, J = 8.0 Hz, 2H, TBNap-H$_3$), 9.05−9.04 (d, J = 4.0 Hz, 4H, pyridyl-H$_\alpha$), 8.97−8.95 (d, J = 8.0 Hz, 2H, TBNap-H$_5$), 8.46 (s, 2H, TBNap-H$_6$), 8.08−8.04 (t, J = 8.0 Hz, 2H, TBNap-H$_4$), 7.91−7.90 (d, J = 4.0 Hz, 4H, Cur-H$_{16}$), 7.88−7.86 (m, 12H, Cur-H$_{17-19}$), 7.27−7.26 (d, J = 4.0 Hz, 4H, pyridyl-H$_\beta$), 6.84−6.80 (d, J = 16.0 Hz, 4H, Cur-H$_{15}$), 6.18−6.16 (d, J = 8.0 Hz, 4H, cymene-H$_{10}$), 5.98−5.96 (d, J = 8.0 Hz, 4H, cymene-H$_9$), 5.81 (s, 2H, Cur-H$_{14}$), 5.62−5.57 (d, J = 20 Hz, 2H, TBNap-H$_7$), 5.03−5.00 (d, J = 12 Hz, 2H, TBNap-H$_{7'}$), 4.95 (s, 2H, TBNap-H$_8$), 4.32 (s, 12H, Cur-OCH_3), 3.41−3.35 (m, 2H, cymene-H$_{13}$), 2.66 (s, 6H, cymene-H$_{11}$), 1.86−1.84 (d, J = 8.0 Hz, 12H, cymene-H$_{12}$); ^{13}C NMR (101 MHz, $CDCl_3$-CD_3OD) δ 178.34, 163.18, 162.58, 152.31, 150.37, 148.66, 147.68, 145.99, 140.38, 131.56, 131.31, 130.10, 128.33, 127.25, 126.92, 126.29, 125.67, 123.19, 122.82, 121.76, 117.28, 115.18, 109.76, 102.91, 98.46, 83.56, 81.88, 65.64, 56.94, 55.43, 30.60, 21.86, 16.92, 14.51. ^{19}F NMR (377 MHz, $CDCl_3$−CD_3OD) δ −79.71 (s, 6F, SO_3CF_3); FT-IR υ_{max} (ATR, cm^{-1}) 2950, 1706, 1669, 1623, 1593, 1507, 1400, 1375, 1341, 1241, 1218, 1158, 1128, 1027, 991, 967, 932, 808, 777, 638, 578.

https://doi.org/10.1021/acs.inorgchem.2c01005
Inorg. Chem. 2022, 61, 11592−11599

RESULTS AND DISCUSSION

Synthesis and Characterization of TBNap. As shown in Scheme 2, **TBNap**, (bis-[*N*-(4-pyridyl)]-9,18-methano-1,8-naphthalimide-[*b*,*f*][1,5]diazocine), was synthesized as a racemic mixture in 54% yield from the precursor **Nap**, *N*-(4-pyridyl)-4-amino-1,8-naphthalimide, which was obtained from *N*-(4-pyridyl)-4-nitro-1,8-naphthalimide by Pd/C catalytic hydrogenation.[29,33] Various spectroscopic techniques were used to characterize **TBNap** (for details, see the Supporting Information). In the ^{1}H NMR spectrum, two doublets and a singlet appeared in the range of δ = 5.16−4.63 ppm due to the $-CH_2-$ proton resonances of the diazocine moiety and the peaks corresponding to the 1,8-naphthalimide and 4-pyridyl moieties appeared at δ = 8.82−7.41 ppm (Figure 1).[26] The HRMS analysis showed an intense peak at m/z = 615.176 ascribed to the molecular ion $[M + H]^+$ (Figure S6).

Scheme 2. Synthesis of TBNap from Precursor Nap

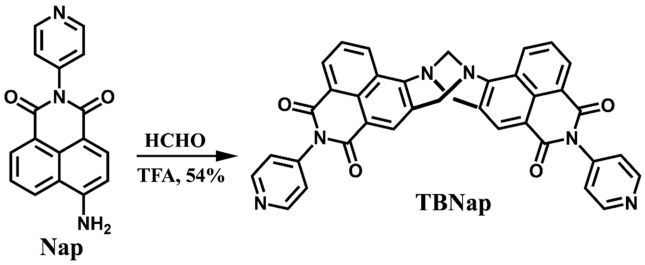

Further, the diffraction analysis was used to elucidate the molecular structure of **TBNap.** The diffraction quality crystals were obtained from the saturated DCM-CH_3OH (2:1) solution of **TBNap** by evaporating at room temperature. Crystallographic details are provided in Table S1. The diffraction analysis revealed that **TBNap** crystallized in monoclinic space group *P*21/c, and the structural model evidenced that the 1,8-naphthalimide units are placed in cleft-shaped confirmation due to the methano-1,5-diazocine ring with the bridgehead angle of 112.25°, and the mean interplanar angle between two 1,8-naphthalimide moieties is 94.68° (Figure 2A). The packing view of **TBNap** showed face-to-face $\pi-\pi$ stacking interactions ($d_{centroid}-d_{centroid}$ = 3.73 Å) between the adjacent ligands, which resulted in head-to-tail arrangements of naphthalimide moieties (Figure 2B). Further,

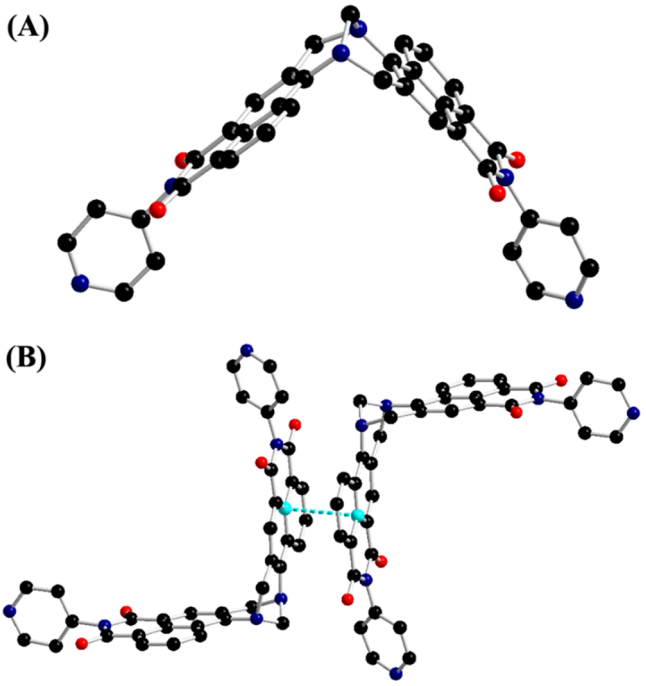

Figure 2. (A) Molecular structure of **TBNap** obtained using diffraction analysis. (B) $\pi-\pi$ stacking interactions (3.73 Å) between two 1,8-naphthalimide moieties. Hydrogen atoms are excluded for clarity (CCDC no. 2121304).

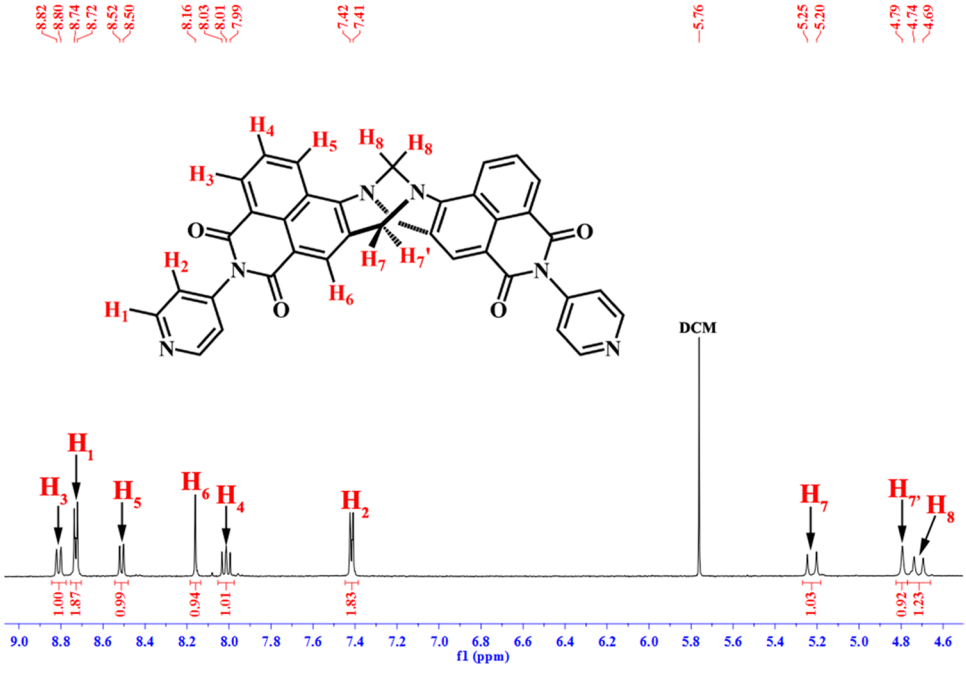

Figure 1. ^{1}H NMR spectrum of **TBNap** (400 MHz, DMSO-d_6) with peak assignment.

https://doi.org/10.1021/acs.inorgchem.2c01005
Inorg. Chem. 2022, 61, 11592−11599

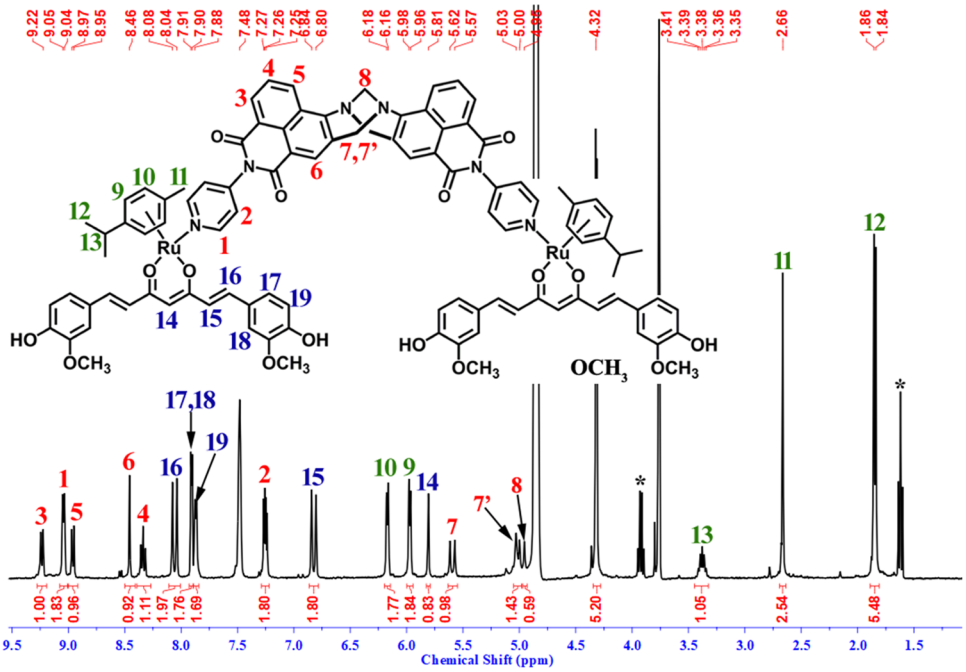

Figure 3. ^{1}H NMR of **TB-Ru-Cur** {400 MHz, $CDCl_3$-CD_3OD (3:1 volume ratio)} with peak assignment. *Peaks of diethyl ether cocrystallized in the recrystallization process.

the solid-state packing diagram of **TBNap** evidenced the presence of multiple C−H···O hydrogen bonding and C−H···π interactions between the adjacent molecules (Figure S7).

Synthesis and Characterization of TB-Ru-Cur. As shown in Scheme 1, **TB-Ru-Cur** was synthesized in a single step *via* metal−ligand coordination assembly. To facilitate the anion exchange, first, **Ru-Cur** (acting as an acceptor) was treated with silver triflate in CH_2Cl_2−CH_3OH (1:1) solution and the anion exchanged **Ru-Cur** was subsequently reacted with the dipyridyl **TBNap** (acting as a donor) in a 2:1 stoichiometry ratio to obtain the expected **TB-Ru-Cur** in 48% yield. **TB-Ru-Cur** was air-stable and highly soluble in common solvents. The *p*-cymene capping moieties engender high structural stability and also limit any further coordination. The coordinated curcuminato ligand further enhances the structural stability *via* the chelate effect. **TB-Ru-Cur** was characterized using Fourier transform infrared (FT-IR), NMR, and electrospray ionization mass spectrometry (ESI-MS) analyses. The FT-IR spectrum showed several intense bands due to the functional groups present in it (see Figure S1). In the ^{1}H NMR spectrum recorded in $CDCl_3$−CD_3OD, the signals for the methylene (−CH_2N−) group of the diazocine moiety appeared as two doublets in the range of 5.62−5.00 ppm, which confirmed the presence of Tröger's base unit (Figure 3). Notably, the peaks corresponding to the 4-pyridyl unit of coordinated **TBNap** were slightly downfield (∼0.3 ppm) shifted compared to the free **TBNap**, which is because of the decrease of electron density upon metal−ligand coordination bonding. The proton signals of *p*-cymene moiety appeared as two sharp doublets at 6.18−5.96 ppm and all the proton resonances due to the curcuminato fragments appearing as sharp signals (Figure 3). The ^{19}F NMR spectrum showed a single peak at δ = 79.71 ppm assigned to the triflate counter anions and the appearance of a single peak also suggested that two triflate anions are chemically equivalent (Figure S9). Furthermore, the appearance of an isotopically well-resolved prominent peak at m/z = 1217.3036 for the charged fragment $[M - (\textbf{RuCur} + OTf^-)]^+$ confirmed the formation of **TB-Ru-Cur** conjugate (Figure S10).

All attempts to obtain the diffraction quality single crystals of **TB-Ru-Cur** were unsuccessful and therefore, computational calculations were conducted to predict the energy-minimized structure. The calculations were conducted using the semi-empirical PM6 method on the Gaussian 09 program.[34] The optimized structure of **TB-Ru-Cur** established a cleft-shaped conformation with the mean interplanar angle between two 1,8-naphthalimide moieties being 103.96°, which is slightly higher than the interplanar angle (94.68°) in free **TBNap** (Figure 4). The two curcuminato units are flanked outward from the cleft and slightly tilted away from the plane of **TBNap** to minimize the steric influence. The two Ru(II) ions adopt a pseudo-octahedral coordination geometry and the distance between them is 22.3 Å. Three coordination sites on each Ru(II) are occupied by the capped *p*-cymene, while the curcuminato ligand coordinates through its two oxygen atoms and the 4-pyridyl "*N*" occupies the sixth coordination site. The two pyridyl-*N* donor sites are coordinated to two different Ru(II) centers, which gives rise to a cleft conformation. The Ru−N bond distance is 2.08 Å, which is slightly less than the Ru−O bond distance of 2.10 Å.

Photophysical Study. We next studied the photophysical properties of **TBNap** and **TB-Ru-Cur** at room temperature (see Figure 5). The absorption and emission spectra were recorded using a 2.5 μM CH_2Cl_2 stock solution. The ultraviolet−visible (UV−vis) absorption spectrum of **TBNap** showed a band at λ = 346 nm (ε = 19.3 × 10^3 M^{-1} cm^{-1}) corresponding to π−π* transition and a band at λ = 387 nm (ε = 23.7 × 10^3 M^{-1} cm^{-1}) assigned to the ICT transition (Figure 5A). Likewise, the absorption spectrum of **TB-Ru-Cur** displayed four typical bands at λ = 347−470 nm (Figure 5A).[26−33] The characteristic metal-to-ligand charge transfer (MLCT) absorption band (due to the transition from the

https://doi.org/10.1021/acs.inorgchem.2c01005
Inorg. Chem. 2022, 61, 11592−11599

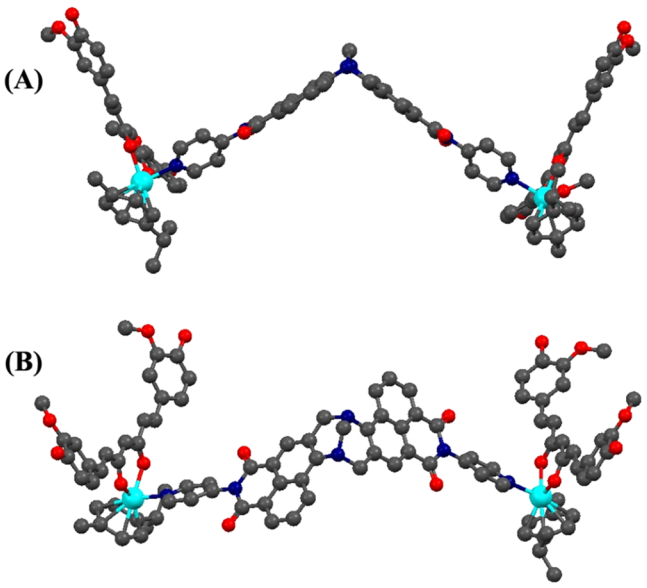

Figure 4. (A) Front and (B) top view of the optimized structure of **TB-Ru-Cur**. Hydrogen atoms are excluded for clarity.

Ru(II) filled 4d orbitals to the empty π^* orbitals of the ligand) appeared at λ = 470 nm (ε = 76.4 × 10^3 M^{-1} cm^{-1}) and the two intense bands at λ = 347 (ε = 55.0 × 10^3 M^{-1} cm^{-1}) and 443 (ε = 86.7 × 10^3 M^{-1} cm^{-1}) are due to the inter/-intramolecular $\pi-\pi^*$ transitions.[24] Notably, the ICT-based absorption band at λ = 400 nm (ε = 105.4 × 10^3 M^{-1} cm^{-1}) was red-shifted by ∼13 nm compared to **TBNap**; this red shift is presumably due to the influence of coordination interactions (Figure 5A). Upon excitation at λ = 387 nm, **TBNap** exhibited an intense ICT emission band at λ = 504 nm, while ICT-based emission of **TB-Ru-Cur** was observed at λ = 511 nm when it was excited at λ = 400 nm (Figure 5B). The ICT-based emission of **TB-Ru-Cur** was slightly red-shifted by 7 nm due to the effect of coordination bonding. The calculated quantum yield for **TBNap** is Φ = 0.242 and 0.135 for **TB-Ru-Cur**. Notably, the emission intensity of **TB-Ru-Cur** was lower than that of **TBNap** emission; this is due to the excited-state energy transfer from **TBNap** to the curcumin moiety, which quenches the emission intensity. The proposed energy transfer process is supported by the absorption and emission spectra overlap of **TB-Ru-Cur**. The existence of an energy transfer in **TB-Ru-Cur** was further supported by the frontiers molecular orbital (highest occupied molecular orbital (HOMO) and lowest unoccupied molecular orbital (LUMO)) diagram obtained from the computational calculations.[34] It is noticed that the highest occupied molecular orbital (HOMO) density was localized on the Ru(II) centers, while the lowest unoccupied molecular orbital (LUMO) density was largely on the 1,8-naphthalimide moieties (Figure S11). These results strongly supported the existence of the proposed MLCT process.

Biological Studies. We next assessed the cellular uptake and antiproliferative activity of **TBNap** and **TB-Ru-Cur** in three different cancer cell lines such as HeLa (cervical cancer), HCT-116 (colon carcinoma), and HepG2 (hepatocellular carcinoma). ICT-based strong fluorescence emission facilitates the visualization of the cellular internalization of compounds using confocal laser scanning microscopy (CLSM). At first, both **TBNap** and **TB-Ru-Cur** were treated separately with HeLa cells and the cells were incubated at different incubation times of 3, 30, and 60 min at 37 °C. Then, the incubated HeLa cells were dosed with a DRAQ5 nuclear stain, and the cells were imaged using CLSM. Due to its nonemissive nature, the cellular internalization of **Ru-Cur** was not able to be visualized. A few representative confocal images of HeLa cells with **TBNap** and **TB-Ru-Cur** at different incubation times are presented in Figure 6. The obtained microscopy images

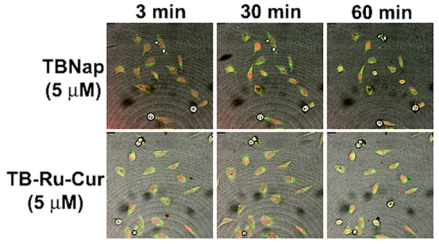

Figure 6. Confocal live-cell images of **TBNap** (5 μM) and **TB-Ru-Cur** (5 μM) within HeLa cells at different incubation times. Green emission = **TBNap** or **TB-Ru-Cur** and red emission = DRAQ5.

exhibited that both **TBNap** and **TB-Ru-Cur** were quickly taken up into cells, even after 3 min of incubation, and localized within the cytoplasm or on the edges of the nucleus. Both **TBNap** and **TB-Ru-Cur** exhibited green emission and the red emission in the nucleus corresponds to the DRAQ5 nuclear stain. However, both **TBNap** and **TB-Ru-Cur** were almost undetectable inside HCT-116 and HepG2 cancer cells probably because of their poor cellular uptake or week emissivity at the concentration of study (Figures S12−S15). Furthermore, the addition of **TB-Ru-Cur** to HepG2 cells seems to harm the cell integrity, where the extracellular membrane is "blebbing" up, suggesting that cells undergo

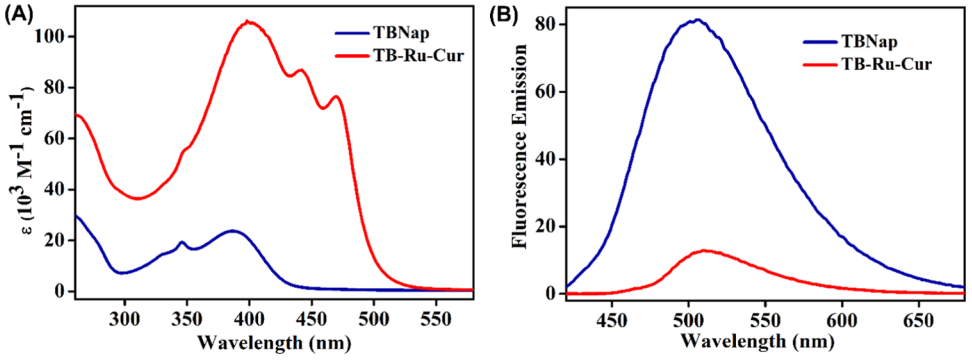

Figure 5. (A) Absorption and (B) emission spectra of **TBNap** and **TB-Ru-Cur** recorded in CH_2Cl_2 (2.5 × 10^{-6} M) at room temperature.

https://doi.org/10.1021/acs.inorgchem.2c01005
Inorg. Chem. 2022, 61, 11592−11599

apoptosis and necrosis (Figure S15).[35] The fast-cellular uptake of **TB-Ru-Cur** can be attributed to its cationic nature, which facilitates enhanced passive diffusion through the cancer cell membrane.[36] The quick cellular internalization and strong fluorescence emission within the HeLa cells endow the application of **TBNap** and **TB-Ru-Cur** as cancer diagnostic probes.

Inspired by the fast-cellular uptake in HeLa cells and cytoplasmic localization, we next assessed the cytotoxicity potential in HCT-116, HeLa, and HepG2 cancer cells for the precursors **TBNap** and **Ru-Cur** as well for the conjugate **TB-Ru-Cur** using the Alamar Blue viability assay. The cancer cells were incubated with different compounds at varying concentrations in the dark for 48 h and then the cell viability was evaluated. The estimated IC_{50} is summarized in Table 1.

Table 1. IC_{50} Values for TBNap, Ru-Cur, and TB-Ru-Cur in HeLa, HCT-116, and HepG2 Cancer Cells

	IC_{50} ± SEM (μM) 48 h incubation in the dark		
ligands and complexes	HeLa	HCT-116	HepG2
TBNap	>100	>100	>100
Ru-Cur	15 ± 3	16 ± 1	16.6 ± 0.6
TB-Ru-Cur	2.0 ± 0.3	2.7 ± 0.1	1.9 ± 0.1
cisplatin	13		

For comparison, the IC_{50} value of the cisplatin drug was measured under identical conditions and included in Table 1. As shown in Figure 7, up to 100 μM concentration of **TBNap** did not induce any cytotoxicity in three cell lines and thus IC_{50} values for **TBNap** were not determined. **Ru-Cur** exhibited moderate cytotoxicity against the three different cell lines and the IC_{50} values estimated were 15 ± 3, 16 ± 1, and 16.6 ± 0.6 μM in HeLa, HCT-116, and HepG2 cells, respectively.

Gratifyingly, the conjugate **TB-Ru-Cur** showed significant cytotoxicity against all three cancer cell lines, being on all occasions significantly more potent than the individual components, with the calculated IC_{50} values of 2.0 ± 0.3, 2.7 ± 0.1, and 1.9 ± 0.1 μM being determined in HeLa, HCT-116, and HepG2, respectively. Notably, the estimated IC_{50} value of **TB-Ru-Nap** was found significantly lower compared to cisplatin (IC_{50} = 13 μM), which was similar to that seen for **Ru-Cur** alone.[37] As Table 1 demonstrates, the anticancer potency of **TB-Ru-Nap** measured in three different cancer cells was significantly higher than that seen for **TBNap** and **Ru-Cur**. The estimated higher anticancer potency of **TB-Ru-Cur** is presumably due to the combined activity of two anticancer agents **Ru-Cur** and **TBNap** motifs, as **TB-Ru-Cur** is significantly more potent than that seen for the individual components. Furthermore, as **TB-Ru-Cur** is highly emissive and easily identifiable within the cellular environment, it makes **TB-Ru-Cur** a potential theragnostic agent in cancer therapy.

CONCLUSIONS

In conclusion, we have synthesized a unique Tröger's base naphthalimide dipyridyl scaffold, **TBNap**, and successfully used it to develop a new *p*-cymene-Ru(II)-curcuminato luminescent conjugate **TB-Ru-Cur**. The structures of **TBNap** and **TB-Ru-Cur** were characterized using standard analytical methods. Further, the molecular structure of the **TBNap** scaffold was elucidated by diffraction analysis. Due to the ICT-based transition, both **TBNap** and **TB-Ru-Cur** were emissive, and thus, using confocal fluorescence microscopy, we have demonstrated the cellular uptake for **TBNap** and **TB-Ru-Cur** both being localized within the cytoplasm of cancer cells. Furthermore, their cytotoxicity potentials against three cancer cell lines were assessed, and cell viability studies showed significantly more anticancer potential for **TB-Ru-Cur** than for the corresponding precursors, with **TBNap** being nontoxic and **Ru-Cur** exhibiting moderate cytotoxicity. In summary, the work discussed herein evidences the versatility of **TBNaps** as potential scaffolds that can be used to generate potential therapeutically active ligands and metal complexes. Further works are in progress to functionalize **TB-Ru-Cur** to improve its selectivity for cancer cells and enhance the anticancer efficacy *via* conjugating the arene-Ru(II) complex to various known bioactive ligands for their applications in cancer therapy.

ASSOCIATED CONTENT

Supporting Information

The Supporting Information is available free of charge at https://pubs.acs.org/doi/10.1021/acs.inorgchem.2c01005.

Details of characterization data {FT-IR, NMR (^{1}H, ^{13}C, and ^{19}F), ESI-MS}, X-ray crystallography, computational simulation, and additional confocal cellular images (PDF)

Accession Codes

CCDC 2121304 contains the supplementary crystallographic data for this paper. These data can be obtained free of charge via www.ccdc.cam.ac.uk/data_request/cif, or by emailing data_request@ccdc.cam.ac.uk, or by contacting The Cambridge Crystallographic Data Centre, 12 Union Road, Cambridge CB2 1EZ, UK; fax: +44 1223 336033.

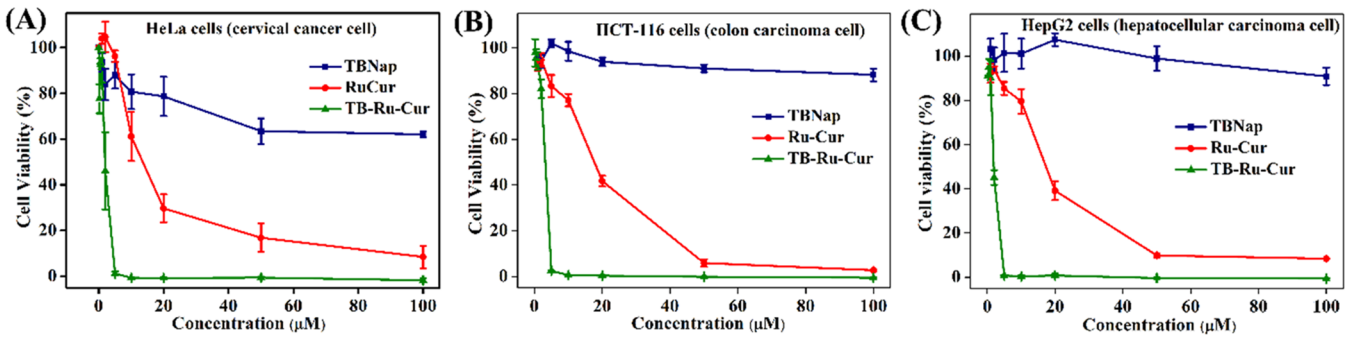

Figure 7. Toxicity profile of **TBNap**, **Ru-Cur**, and **TB-Ru-Cur** in (A) HeLa, (B) HCT-116, and (C) HepG2 cancer cells.

https://doi.org/10.1021/acs.inorgchem.2c01005
Inorg. Chem. 2022, 61, 11592−11599

AUTHOR INFORMATION

Corresponding Authors

Thorfinnur Gunnlaugsson − *School of Chemistry and Trinity Biomedical Sciences Institute, Trinity College Dublin, The University of Dublin, Dublin 2 D02 PN40, Ireland;* orcid.org/0000-0003-4814-6853; Email: gunnlaut@tcd.ie

Sankarasekaran Shanmugaraju − *Department of Chemistry, Indian Institute of Technology Palakkad, Palakkad 678557 Kerala, India;* orcid.org/0000-0002-3283-7847; Email: shanmugam@iitpkd.ac.in

Authors

Binduja Mohan − *Department of Chemistry, Indian Institute of Technology Palakkad, Palakkad 678557 Kerala, India*

Sandra Estalayo-Adrián − *School of Chemistry and Trinity Biomedical Sciences Institute, Trinity College Dublin, The University of Dublin, Dublin 2 D02 PN40, Ireland*

Deivasigamani Umadevi − *Department of Chemistry, Indian Institute of Technology Palakkad, Palakkad 678557 Kerala, India;* orcid.org/0000-0001-9732-2556

Bjørn la Cour Poulsen − *School of Chemistry and Trinity Biomedical Sciences Institute, Trinity College Dublin, The University of Dublin, Dublin 2 D02 PN40, Ireland*

Salvador Blasco − *Instituto de Ciencia Molecular, Universidad de Valencia, 46980 Paterna, Spain*

Gavin J. McManus − *School of Biochemistry and Immunology and Trinity Biomedical Sciences Institute, Trinity College Dublin, The University of Dublin, Dublin 2 D02 PN40, Ireland*

Complete contact information is available at: https://pubs.acs.org/10.1021/acs.inorgchem.2c01005

Notes

The authors declare no competing financial interest.

ACKNOWLEDGMENTS

The authors are grateful to the Science and Engineering Research Board (EMEQ Award EEQ/2018/000799 to S.S.) and Science Foundation Ireland (SFI PI Awards 10/45 IN.1/B2999 and 13/IA/1865 to T.G.) for the financial support. S.B. thanks ERC for a Marie Curie grant. B.M. and S.S. are thankful to the Department of Chemistry and CIF-CMFF, IIT Palakkad, for providing the characterization facilities.

REFERENCES

(1) (a) Poynton, F. E.; Bright, S. A.; Blasco, S.; Williams, D. C.; Kelly, J. M.; Gunnlaugsson, T. The Development of Ruthenium(II) Polypyridyl Complexes and Conjugates for In-vitro Cellular And In-vivo Applications. *Chem. Soc. Rev.* **2017**, *46*, 7706−7756. (b) Bhat, I. A.; Jain, R.; Siddiqui, M. M.; Saini, D. K.; Mukherjee, P. S. Water-Soluble Pd_8L_4 Self-assembled Molecular Barrel as an Aqueous Carrier for Hydrophobic Curcumin. *Inorg. Chem.* **2017**, *56*, 5352−5360.

(2) Siegel, R. L.; Miller, K. D.; Fuchs, H. E.; Jemal, A. Cancer Statistics, 2021. *Ca-Cancer J. Clin.* **2021**, *71*, 7−33.

(3) Mansoori, B.; Mohammadi, A.; Davudian, S.; Shirjang, S.; Baradaran, B. The Different Mechanisms of Cancer Drug Resistance: A Brief Review. *Adv. Pharm. Bull.* **2017**, *7*, 339−348.

(4) Dallavalle, S.; Dobričić, V.; Lazzarato, L.; Gazzano, E.; Machuqueiro, M.; Pajeva, I.; Tsakovska, I.; Zidar, N.; Fruttero, R. Improvement of Conventional Anti-Cancer Drugs as New Tools against Multidrug Resistant Tumors. *Drug Resistance Updates* **2020**, *50*, No. 100682.

(5) Zeng, L.; Gupta, P.; Chen, Y.; Wang, E.; Ji, L.; Chao, H.; Chen, Z.-S. The Development of Anti-cancer Ruthenium(II) Complexes: From Single Molecule Compounds to Nanomaterials. *Chem. Soc. Rev.* **2017**, *46*, 5771−5804.

(6) Wanninger, S.; Lorenz, V.; Subhan, A.; Edelmann, F. T. Metal Complexes of Curcumin − Synthetic Strategies, Structures and Medicinal Applications. *Chem. Soc. Rev.* **2015**, *44*, 4986−5002.

(7) Štarha, P.; Trávníček, Z. Non-Platinum Complexes Containing Releasable Biologically Active Ligands. *Coord. Chem. Rev.* **2019**, *395*, 130−145.

(8) Zheng, Y.-R.; Suntharalingam, K.; Johnstone, T. C.; Lippard, S. J. Encapsulation of Pt(IV) Prodrugs within a Pt(II) Cage For Drug Delivery. *Chem. Sci.* **2015**, *6*, 1189−1193.

(9) Bratsos, I.; Jedner, S.; Gianferrara, T.; Alessio, E. Ruthenium Anticancer Compounds: Challenges and Expectations. *Chimia* **2007**, *61*, 692−697.

(10) Hartinger, C. G.; Jakupec, M. A.; Zorbas-Seifried, S.; Kynast, B.; Zorbas, H.; Keppler, B. K.; et al. KP1019, A New Redox-Active Anticancer Agent–Preclinical Development and Results of a Clinical Phase I Study in Tumor Patients. *Chem. Biodiversity* **2008**, *5*, 2140−2155.

(11) Reedijk, B. J. Metal-Ligand Exchange Kinetics in Platinum and Ruthenium Complexes. *Platinum Met. Rev.* **2008**, *52*, 2−11.

(12) Dyson, P. J.; Sava, G. J. Metal-based Antitumour Drugs in the Post Genomic Era. *Dalton Trans.* **2006**, 1929−1933.

(13) Dougan, S. J.; Sadler, P. J. The Design of Organometallic Ruthenium Arene Anticancer Agents. *Chimia* **2007**, *61*, 704−715.

(14) Süss-Fink, G. Areneruthenium Complexes as Anticancer Agents. *Dalton Trans.* **2010**, *39*, 1673−1688.

(15) Hayward, R. L.; Schornagel, Q. C.; Tente, R.; Macpherson, J. S.; Aird, R.; Guichard, S.; Habtemariam, A.; Sadler, P. J.; OJodrell, D. I. Investigation of the Role of Bax, P21/Waf1 and P53 as Determinants of Cellular Responses in HCT116 Colorectal Cancer Cells Exposed to the Novel Cytotoxic Ruthenium(II) Organometallic Agent, RM175. *Cancer Chemother. Pharmacol.* **2005**, *55*, 577−583.

(16) Seršen, S.; Kljun, J.; Kryeziu, K.; Panchuk, R.; Alte, B.; Körner, W.; Heffeter, P.; Berger, W.; Turel, I. Structure-Related Mode-of-Action Differences of Anticancer Organoruthenium Complexes with β-Diketonates. *J. Med. Chem.* **2015**, *58*, 3984−3996.

(17) (a) Pröhl, M.; Ulrich, S. S.; Weigand, W.; Gottschaldt, M. Metal complexes of curcumin and curcumin derivatives for molecular imaging and anticancer therapy. *Coord. Chem. Rev.* **2016**, *307*, 32−41. (b) Murphy, S. A.; Phelan, C.; Shanmugaraju, S.; Blascoc, S.; Gunnlaugsson, T. Fluorescent 3-amino-1,8-naphthalimide Tröger's Bases (3-Amino-TBNaps) Incorporating Protected α-Amino Acids. *Tetrahedron Lett.* **2021**, *83*, No. 153405. (c) Murphy, S. A.; Phelan, C. A.; Veale, E. B.; Kotova, O.; Comby, S.; Gunnlaugsson, T. Fluorescent 4-amino-1,8-naphthalimide Tröger's Bases (TBNaps) Possessing (Orthogonal) "α -Amino Acids," Esters and Di-Peptides and their Solvent Dependent Photophysical Properties. *Org. Biomol. Chem.* **2021**, *19*, 6817−6833.

(18) Grynkiewicz, G.; Ślifirski, P. Curcumin and Curcuminoids in Quest for Medicinal Status. *Acta Biochim. Pol.* **2012**, *59*, 201−212.

(19) Banerjee, S.; Chakravarty, A. R. Metal Complexes of Curcumin for Cellular Imaging, Targeting, and Photoinduced Anticancer Activity. *Acc. Chem. Res.* **2015**, *48*, 2075−2083.

(20) Esatbeyoglu, T.; Huebbe, P.; Ernst, I.M.A.; Chin, D.; Wagner, A. E.; Rimbach, G. Curcumin-from Molecule to Biological Function. *Angew. Chem., Int. Ed.* **2012**, *51*, 5308−5332.

(21) Shen, L.; Ji, H.-F. The Pharmacology of Curcumin: is it the Degradation Products? *Trends Mol. Med.* **2012**, *18*, 138−144.

(22) Caruso, F.; Rossi, M.; Benson, A.; Opazo, C.; Freedman, D.; Monti, E.; Gariboldi, M. B.; Shaulky, J.; Marchetti, F.; Pettinari, R.; Pettinari, C. Ruthenium-arene Complexes of Curcumin: X-ray and Density Functional Theory Structure, Synthesis, and Spectroscopic Characterization, In-vitro Antitumor Activity, and DNA Docking Studies of (p-cymene)Ru(curcuminato)chloro. *J. Med. Chem.* **2012**, *55*, 1072−1081.

(23) Pettinari, R.; Marchetti, F.; Condello, F.; Pettinari, C.; Lupidi, G.; Scopelliti, R.; Mukhopadhyay, S.; Riedel, T.; Dyson, P. J. Ruthenium (II)−Arene RAPTA Type Complexes containing Curcumin and Bisdemethoxycurcumin display Potent and Selective Anticancer Activity. *Organometallics* **2014**, *33*, 3709−3715.
(24) Shanmugaraju, S.; Poulsen, B.L.C.; Arisa, T.; Umadevi, D.; Dalton, H. L.; Hawes, C. S.; Estalayo-Adrián, S.; Savyasachi, A. J.; Watson, G. W.; Williams, D. C.; Gunnlaugsson, T. Synthesis, Structural Characterisation and Antiproliferative Activity of a New Fluorescent 4-amino-1,8-naphthalimide Tröger's Base−Ru(II)−Curcumin Organometallic Conjugate. *Chem. Commun.* **2018**, *54*, 4120−4123.
(25) (a) Shanmugaraju, S.; McAdams, D.; Pancotti, F.; Hawes, C. S.; Veale, E. B.; Kitchen, J. A.; Gunnlaugsson, T. One-Pot Facile Synthesis of 4-amino-1,8-naphthalimide derived Tröger's Bases via a Nucleophilic Displacement Approach. *Org. Biomol. Chem.* **2017**, *15*, 7321−7329. (b) Calatrava-Pérez, E.; Acherman, S.; Stricker, L.; McManus, G.; Delente, J.; Lynes, A. D.; Henwood, A. F.; Lovitt, J. I.; Hawes, C. S.; Byrne, K.; Schmitt, W.; Kotova, O.; Gunnlaugssona, T.; Scanlan, E. M. Fluorescent Supramolecular Hierarchical Self-Assemblies from Glycosylated 4-amino- and 4-bromo-1,8-naphthalimides. *Org. Biomol. Chem.* **2020**, *18*, 3475−3480.
(26) (a) Shanmugaraju, S.; Dabadie, C.; Byrne, K.; Savyasachi, A. J.; Umadevi, D.; Schmitt, W.; Kitchen, J. A.; Gunnlaugsson, T. A Supramolecular Tröger's base derived Coordination Zinc Polymer for Fluorescent Sensing of Phenolic-Nitroaromatic Explosives in Water. *Chem. Sci.* **2017**, *8*, 1535−1546. (b) Binduja, M.; Prabukumar, B.; Umadevi, D.; Shanmugaraju, S. A Simple 4-Amino-1,8-Naphthalimide Hydrazine based "Turn-On" Fluorescent Chemosensor for Selective and Reversible Detection of Zn(II) Ion. *Inorg. Chim. Acta* **2022**, *533*, No. 120798.
(27) Veale, E. B.; Frimannsson, D. O.; Lawler, M.; Gunnlaugsson, T. 4-Amino-1,8-naphthalimide-based Tröger's Bases as High Affinity DNA Targeting Fluorescent Supramolecular Scaffolds. *Org. Lett.* **2009**, *11*, 4040−4043.
(28) Banerjee, S.; Bright, S. A.; Smith, J. A.; Burgeat, J.; Martinez-Calvo, M.; Williams, D. C.; Kelly, J. M.; Gunnlaugsson, T. A Supramolecular Approach to Enantioselective DNA Recognition using Enantiomerically Resolved Cationic 4-Amino-1,8-Naphthalimide based Tröger s Base. *J. Org. Chem.* **2014**, *79*, 9272−9283.
(29) Shanmugaraju, S.; Hawes, C. S.; Savyasachi, A. J.; Blasco, S.; Kitchen, J. A.; Gunnlaugsson, T. Supramolecular Coordination Polymers using a Close to 'V-Shaped' Fluorescent 4-amino-1,8-naphthalimide Tröger's Base Scaffold. *Chem. Commun.* **2017**, *53*, 12512−12515.
(30) Delente, J. M.; Umadevi, D.; Shanmugaraju, S.; Kotova, O.; Watson, G. W.; Gunnlaugsson, T. Aggregation Induced Emission (AIE) Active 4-amino-1,8-naphthalimide-Tröger's Base for the Selective Sensing of Chemical Explosives in Competitive Aqueous Media. *Chem. Commun.* **2020**, *56*, 2562−2565.
(31) Shanmugaraju, S.; Umadevi, D.; Barcia, L.M.G.; Delente, J. M.; Byrne, K.; Schmitt, W.; Watson, G. W.; Gunnlaugsson, T. "Turn-on" Fluorescence Sensing of Volatile Organic Compounds using a 4-amino-1,8-naphthalimide Tröger's Base Functionalised Triazine Organic Polymer. *Chem. Commun.* **2019**, *55*, 12140−12143.
(32) Delente, J. M.; Umadevi, D.; Byrne, K.; Schmitt, W.; Watson, G. W.; Gunnlaugsson, T.; Shanmugaraju, S. Hyper-Crosslinked 4-amino-1,8-naphthalimide Tröger's Base containing Pyridinium Covalent Organic Polymer (COP) for Discriminative Fluorescent Sensing of Chemical Explosives. *Supramol. Chem.* **2020**, *32*, 508−517.
(33) Lovitt, J. I.; Umadevi, D.; Rajalakshmi, P.; Twamley, B.; Gunnlaugsson, T.; Shanmugaraju, S. Synthesis, Structural Characterization, Antibiotics Sensing and Coordination Chemistry of a Fluorescent 4-amino-1,8-naphthalimide Tröger's Base Supramolecular Scaffold. *Supramol. Chem.* **2020**, *32*, 620−633.
(34) Frisch, M. J.; Trucks, G. W.; Schlegel, H. B.; Scuseria, G. E.; Robb, M. A.; Cheeseman, J. R.; Scalmani, G.; Barone, V.; Mennucci, B.; Petersson, G. A.; Nakatsuji, H.; Caricato, M.; Li, X.; Hratchian, H. P.; Izmaylov, A. F.; Bloino, J.; Zheng, G.; Sonnenberg, J. L.; Hada, M.; Ehara, M.; Toyota, K.; Fukuda, R.; Hasegawa, J.; Ishida, M.; Nakajima, T.; Honda, Y.; Kitao, O.; Nakai, H.; Vreven, T.; Montgomery, J. A.; Peralta, J. E.; Ogliaro, F.; Bearpark, M.; Heyd, J. J.; Brothers, E.; Kudin, K. N.; Staroverov, V. N.; Kobayashi, R.; Normand, J.; Raghavachari, K.; Rendell, A.; Burant, J. C.; Iyengar, S. S.; Tomasi, J.; Cossi, M.; Rega, N.; Millam, J. M.; Klene, M.; Knox, J. E.; Cross, J. B.; Bakken, V.; Adamo, C.; Jaramillo, J.; Gomperts, R.; Stratmann, R. E.; Yazyev, O.; Austin, A. J.; Cammi, R.; Pomelli, C.; Ochterski, J. W.; Martin, R. L.; Morokuma, K.; Zakrzewski, V. G.; Voth, G. A.; Salvador, P.; Dannenberg, J. J.; Dapprich, S.; Daniels, A. D.; Farkas; Foresman, J. B.; Ortiz, J. V.; Cioslowski, J.; Fox, D. J. *Gaussian 09*, Revision A.02; Gaussian, Inc.: Wallingford CT, 2009.
(35) Poon, I. K. H.; Lucas, C. D.; Rossi, A. G.; Ravichandran, K. S. Apoptotic Cell Clearance: Basic Biology and Therapeutic Potential. *Nat. Rev. Immunol.* **2014**, *14*, 166−180.
(36) Ryan, G. J.; Elmes, R.B.P.; Erby, M.-L.; Poynton, F. E.; Williams, D. C.; Quinna, S. J.; Gunnlaugsson, T. Unexpected DNA Binding Properties with Correlated Downstream Biological Applications in Mono *Vs.* Bis-1,8-naphthalimide Ru(II)-polypyridyl Conjugates. *Dalton. Trans.* **2015**, *44*, 16332−16344.
(37) Tardito, S.; Isella, C.; Medico, E.; Marchio, L.; Bevilacqua, E.; Hatzoglou, M.; Bussolati, O.; Franchi-Gazzola, R. The Thioxotriazole Copper(II) Complex A0 Induces Endoplasmic Reticulum Stress and Paraptotic Death in Human Cancer Cells. *J. Biol. Chem.* **2009**, *284*, 24306−24319.

https://doi.org/10.1021/acs.inorgchem.2c01005
Inorg. Chem. 2022, 61, 11592−11599